Fluorescence lidar imaging of historical monuments

Weibring, Petter; Johansson, Thomas; Edner, Hans; Svanberg, Sune; Sundner, B; Raimondi, V; Cecchi, G; Pantani, L

Published in:
Applied Optics

DOI:
10.1364/AO.40.006111

2001

Fluorescence lidar imaging of historical monuments

Petter Weibring, Thomas Johansson, Hans Edner, Sune Svanberg, Barbro Sundnér, Valentina Raimondi, Giovanna Cecchi, and Luca Pantani

What is believed to be the first fluorescence imaging of the facades of a historical building, which was accomplished with a scanning fluorescence lidar system, is reported. The mobile system was placed at a distance of ~60 m from the medieval Lund Cathedral (Sweden), and a 355-nm pulsed laser beam was swept over the stone facades row by row while spectrally resolved fluorescence signals of each measurement point were recorded. By multispectral image processing, either by formation of simple spectral-band ratios or by use of multivariate techniques, areas with different spectral signatures were classified. In particular, biological growth was observed and different stone types were distinguished. The technique can yield data for use in facade status assessment and restoration planning. © 2001 Optical Society of America

OCIS codes: 100.2960, 120.0280, 260.2510, 280.3640, 300.2530.

1. Introduction

Historical buildings constitute an important component of our cultural heritage. However, extensive control of their status and their conservation can often be troublesome and time-consuming tasks. From this point of view, the use of remote-sensing techniques may be an attractive method for quick and truly nondestructive monitoring of building surfaces. Color photography is one obvious approach; however, fluorescence techniques are known to be capable of revealing aspects that are not evident to the naked eye or to photography. The use of fluorescence in forensic science,[1] art inspection,[2] and tissue diagnostics[3] is well known. All these applications are carried out in indoor, controlled environments, although sometimes competing background light, e.g., surgical lamps, make pulsed excitation and time-gated detection necessary.[4]

Fluorescence lidar techniques[5] make it possible to extend the application of fluorescence spectroscopy to the outdoor environment (remote sensing), where large distances and uncontrollable background light have to be dealt with. Point-monitoring fluorescence lidars have been used extensively for aquatic monitoring[5–8] and for studies of terrestrial vegetation.[9,10] More recently, the same techniques were used for point monitoring of stone facades of historical monuments.[11]

The possibility of remote fluorescence imaging was demonstrated on plants and on parts of trees, the laser-illuminated scene was captured simultaneously in four spectral bands.[12,13] This technique cannot be extended to large targets, at least not for a reasonable laser power, because of the competition between background daylight and the energy density of fluorescence light from the target. A push-broom type of lidar, in which the available excitation radiation is spread out as a horizontal streak, was also successfully developed. Fluorescence imaging at a distance of 50 m was demonstrated by scanning of a tree from its roots to the canopy.[14]

When even larger objects, such as buildings, are to be imaged in fluorescence, even the push-broom technique is not adequate, because spreading the laser light over too large a line produces unfavorable signal-to-background ratio conditions. In this case, a scanning technique seems to be the most suitable one. The laser beam is concentrated in a high-intensity spot on the target, which can be placed at a considerable distance from it and is observed by the receiving system with a narrow field of view. The received light can then be dispersed by a spectrome-

P. Weibring, Th. Johansson, H. Edner, and S. Svanberg (e-mail: sune.svanberg@fysik.lth.se) are with the Department of Physics, Lund Institute of Technology, P.O. Box 118, S-221 00 Lund, Sweden. B. Sundnér is with the Central Board for National Antiquities, S-114 84 Stockholm, Sweden. When this research was performed, V. Raimondi, G. Cecchi, and L. Pantani were with the Istituto di Ricerca sulle Onde Elettromagnetiche "Nello Carrara," Consiglio Nazionale delle Richerche, Via Panciatichi 64, I-50127 Florence, Italy.

Received 7 March 2001; revised manuscript received 23 July 2001.

0003-6935/01/336111-10$15.00/0

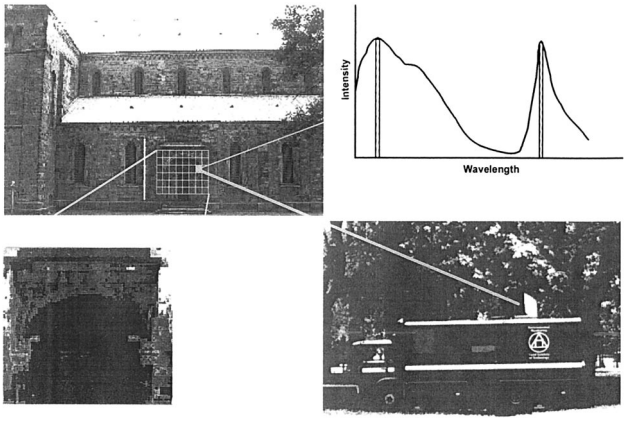

Fig. 1. Fluorescence lidar multispectral imaging at a historical building. Top left, photograph of the northern facade of the Lund Cathedral, with the portal area studied in the present research indicated. A specially selected vertical scan line is also indicated. Bottom right, photograph of the Swedish mobile lidar system during the fluorescence imaging measurements. Top right, single-point remote fluorescence spectrum for the facade. Filter bands are shown by hatched regions. Bottom left, fluorescence image of the 8 m × 8 m marked area covering the northern portal. The image was recorded at 682 nm and displays biodeteriogen colonization.

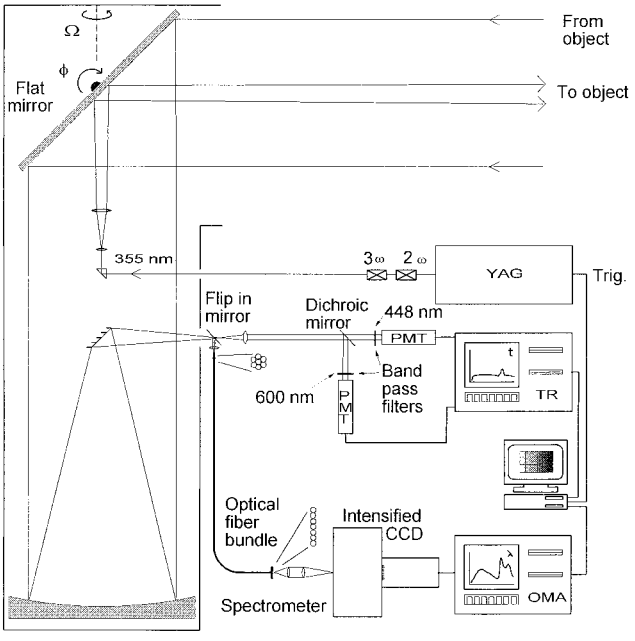

Fig. 2. Optical and electronic arrangement of the lidar system employed in measurements of the historic building. PMTs, photomultiplier tubes; OMA, optical multichannel analyzer; TR, transient digitizer.

ter and detected by a normal gated and intensified optical multichannel analyzer. With this procedure, a high signal-to-noise ratio can be obtained. If high spatial resolution is required, the scanning technique with a small laser spot on target requires quite a long recording time. This restriction poses no fundamental problems in building analysis because the targets are fixed ones.

A preliminary experiment was performed on a 1 m × 1 m arrangement of stones of different origins that employs two fluorescence bands selected with interference filters and by photomultiplier detection.[15] In the present paper, we report a fluorescence remote-sensing study of a large building, the medieval Lund Cathedral, by multispectral fluorescence techniques. It is believed that this is the first fluorescence multispectral imaging of a historic monument. The measurement method, including photographs of the northern facade of the cathedral and a fluorescence lidar system in measuring position, is shown in Fig. 1.

2. Experimental Techniques

A mobile lidar laboratory,[16,17] which is adapted primarily for atmospheric monitoring by the differential absorption technique, was employed for the experiments. However, the system has a flexible design and previously was used in monitoring remote fluorescence.[8,9,12–15,18] The optical and electronic configurations employed in the present experiments are shown in Fig. 2.

The fluorescence lidar transmitter was a frequency-tripled Nd:YAG laser generating radiation at 355 nm in 8-ns-long pulses at a repetition rate of 20 Hz. Typically the transmitted pulse energy was limited to 30 mJ in these experiments. The vertically looking receiving optics was a Newtonian telescope with a 40-cm diameter. A 40 cm × 80 cm folding mirror was placed over the telescope in a dome above the vehicle roof. A mirror directed the laser beam and the coaxial telescope's field of view to the measurement point, employing stepping motor control of the mirror. Two parallel detection systems were used. The first one was based on filters and photomultipliers. The fluorescence light was split up into two arms by a dichroic beam splitter, and two spectral bands of 10 nm-width were selected by interference filters, either at 438 and 682 nm or at 448 and 600 nm. The two fluorescence signals were then integrated with an appropriate time gate placed over the fluorescence lidar echoes recorded with a two-channel transient digitizer. The second system permitted a recording of the full spectrum with high spectral resolution. A gated and intensified optical multichannel analyzer detected the fluorescence radiation from 440 to 740 nm with a spectral resolution of ~10 nm. The laser beam expander, which was coaxial with the receiving telescope, was normally adjusted to give an 8-cm-diameter laser spot on the target. For a typical distance of 60 m between the lidar and the target, the diameter of the image spot in the telescope focal plane was ~1.3 mm. A special fiber bundle, which contained seven individual fibers densely packed in a circle, captured the focal image spot. The bundle output was rearranged into a linear shape that matched the input slit of the spectrometer.

With the computer-controlled folding mirror the lidar was pointed at selected points for spectral data

collection or scanned row by row the facades for image generation. A signal integration of eight laser shots was normally used. Data storage and mirror advancement to the next measurement point took less than 1 s. Daytime measurements with high spectral resolution were possible through the detector time-gating technique with a 100-ns-wide gate set to open in coincidence with the arrival time of the fluorescence pulse.

Spectral calibration of the wavelength-resolved system was not performed. However, as we are interested mostly in differences in spectral signatures among different areas rather than in absolute shapes, and because some noise is introduced in the process, spectral correction was not implemented for the data presented in this paper.

3. Field Experiment

The Lund Cathedral, the largest Romanesque building in northern Europe, was constructed mostly in the early 12th century. However, it has been rebuilt several times. More recently, during the period 1833–1880 the cathedral was partly rebuilt and restored. The old western towers were replaced by the existing ones in the 1880s.

The main stone masonry consists of ashlars made from a dense quartzitic sandstone, quarried in the Höör area northeast of Lund. This sandstone is generally highly resistant to weathering. However, it undergoes a color change when it is exposed to the atmosphere, resulting in a thin black staining. The same sandstone was used as a building material in both in the 12th and the 19th centuries. There is, however, a difference: In the 19th century a harder and denser type was used. Certain areas of the exposed facade are made from sandstone quarried in the 12th century, whereas others are constructed with sandstone from the 19th century. In the renovations and reconstruction, older and newer stones have sometimes been mixed. The fundament was partly reconstructed with granite in the 19th century.

In connection with investigations of the building materials, damage to the stone material has also been examined. On the exterior walls of the cathedral, black staining, salt efflorescence, exfoliation, and biodeteriogen colonization (algae, lichens) have been investigated.[19–21] This situation provides a challenge for testing fluorescence techniques for the determination of various biodeteriogens and stone types and their extension.

The one-week measurement campaign was held in late October 1997. The weather was unsettled, with occasional snowfall and temperatures a few degrees above freezing. Inasmuch as the laser-beam scans frequently started at ground level, the measurement area was blocked off. It should be noted that with an 8-cm laser spot size on target the 355-nm beam is eye safe according to current regulations.

Most measurements were concentrated on the northern portal, but also other parts of the building, such as the upper walls and the towers, were studied. The area close to the northern portal is shown in Fig. 1, together with a point fluorescence spectrum and a fluorescence image of the portal area (marked in the photo) recorded through a 682-nm filter. The positioning of the lidar at a minimum distance of 60 m from the northern facade gave the laser beam access to all the areas under investigation without serious geometrical distortion of the detected images.

4. Measurements and Analysis

Spectra of laser-induced fluorescence pertaining to stone and mineral samples were discussed previously.[11,15,22–24] In this experiment three measurement modes were employed. First, single-point spectra were detected on different stone types and different biodeteriogens, in parallel with visual identification. A spectral library was built with these spectra and used for identification purposes in later measurements. In the second mode, vertical and horizontal scans, recording high-resolution spectra, were performed on the upper and side parts of the northern portal and on other parts of the facades.

In the last mode, fluorescence images were acquired by use of either the band filters or the spectrometer system. At the northern portal of the cathedral, an area of 8 m $\times$ 8 m was investigated in detail. Both a two-wavelength image and a high-spectral-resolution image, each one containing 6400 pixels, were acquired during 2-h-long runs. The images show different stone types and occasional biodeteriogen colonization. Unfortunately, exact records of the positions of the biological samples collected for analysis were not noted, and this complicates unambiguous biological identification of the recorded fluorescence images.

A. Point Monitoring

Point monitoring was performed at the northern portal, at some of the northern facade pilasters, and at other individual points. An observer, close to the facade, selected the measurement points and by radio communication directed the lidar operator, who activated the stepping motors of the steering mirror to bring the laser beam into position. Each motor step resulted in a position shift on the target of $\sim$0.4 cm horizontally and $\sim$1.1 cm vertically.

The northern portal is shown enlarged in Fig. 3, with some examples of fluorescence spectra at selected positions. Spectral signatures of different types of surface can be identified. The three spectra at the left belong to sandstones. The lowest of these spectra corresponds to a comparatively clean 19th-century stone; the middle one originates from a stone with a thin layer of biodeteriogens not distinguishable by visual inspection. This spectrum is clearly distinguished from that of the clean stone by the chlorophyll fluorescence in the red. The top left spectrum corresponds to sandstone covered by a dark crust. The spectrum at the center right of the picture shows the spectral signature from a stone with a stronger red signal. At this location it was also possible to identify biodeteriogen colonization with the naked eye. This comparison already confirms[25] the

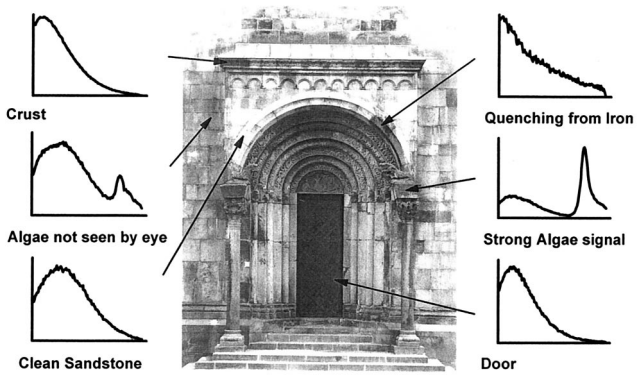

Fig. 3. Photograph of the northern portal and representative remotely recorded point-monitoring fluorescence spectra. The spectra are normalized in intensity and are shown for wavelengths from 440 to 740 nm.

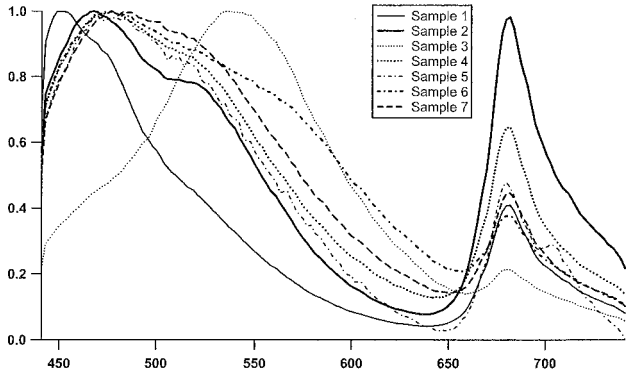

Fig. 5. Point monitoring spectra of different types of biodeteriogen colonization on the cathedral facade. The spectra were recorded by accumulation of 20 laser shots at 60-m distance and are intensity normalized.

capabilities of the fluorescence technique for the early identification, mapping, and control of biodeteriogen colonization. At the upper right of Fig. 3 the spectral signature of sandstone with rust on its surface is shown. The rust is due to a protruding iron bar, positioned for wall reinforcement. The fluorescence from the sandstone is quenched here by the iron ions,[26] giving a clear fingerprint of the facade areas influenced by the presence of iron. Figure 3 also includes the signature of the black-painted wooden door at the lower right.

A more systematic study of the different types of stone and biodeteriogen spectra is presented in Figs. 4 and 5. Figure 4 displays laser-induced fluorescence spectra of two different types of reasonably clean sandstone, of sandstone with a dark crust, of iron-quenched sandstone fluorescence, and finally, of a yellowish type of stone that is sparsely used in the facade. Spectra are shown both with the recorded intensity obtained for a fixed excitation pulse energy (top) and with intensity normalization (bottom), thus permitting better comparisons of the spectral shapes. None of the stones studied exhibited the typical chlorophyll fluorescence spectral signature; however, those stones are not clean stones but rather stones with natural surface aging, salt crust formation, and pollution deposition. The center positions of the transmission bands of the two filters, at 600 and 448 nm, employed in the lidar detection system for some

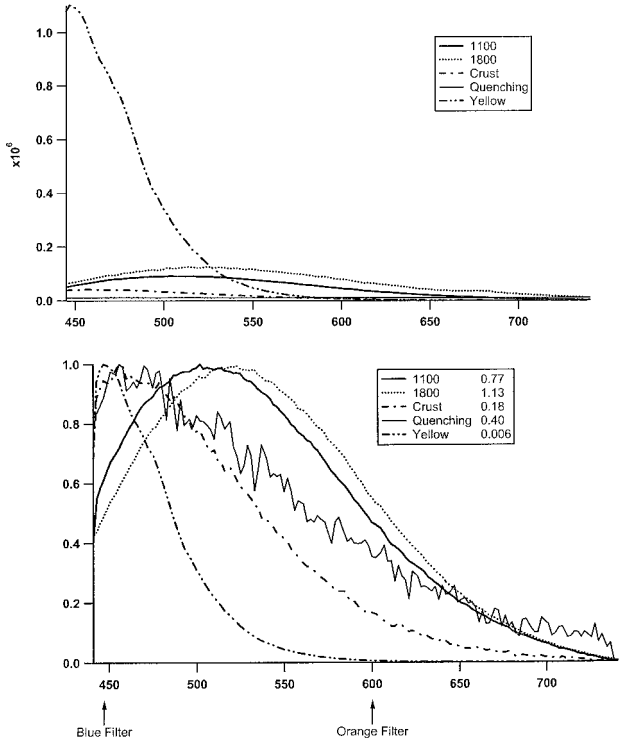

Fig. 4. Point-monitoring spectra of different types of stone in the cathedral facade. The spectra were recorded by accumulation of 20 shots at 60-m distance. Spectra are given with the detected intensities (top) and normalized to their maximum value (bottom). The generic spectral shapes of 12th- and 19th-century sandstone, stones with a crust, stones affected by quenching rust (iron ions), and a rarely occurring yellowish facade stone are given. In the normalized spectra, the intensity ratios for the signal levels at the orange (600-nm) and the blue (448-nm) filters used are also given.

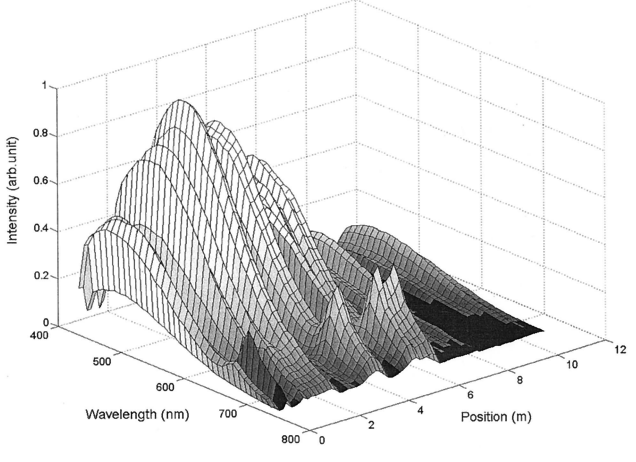

Fig. 6. Fluorescence spectra for an 11-m vertical line scan on the left side of the northern portal as indicated in Fig. 1. Spectra are shown in a three-dimensional surface plot.

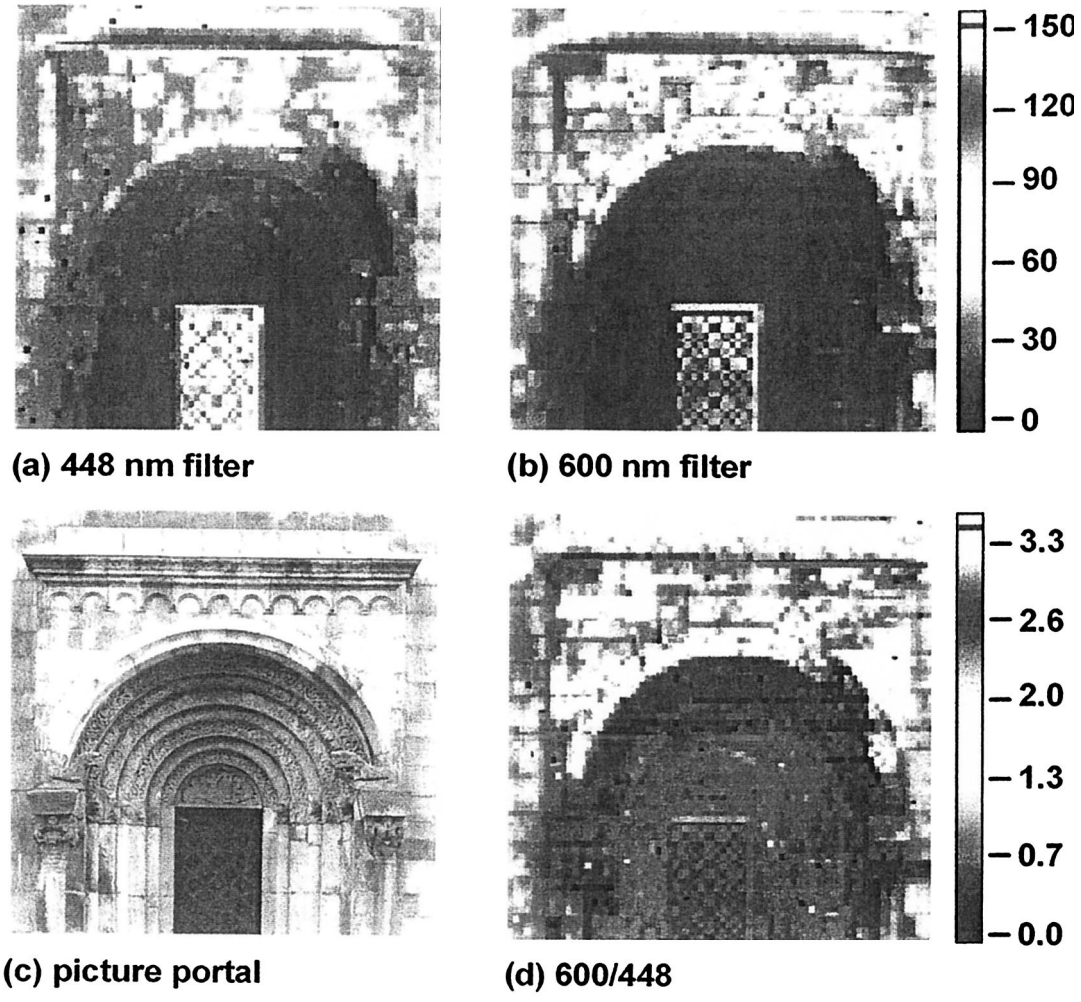

Fig. 7. Simultaneous recording of fluorescence images taken through (a) 448- and (b) 600-nm filters (two-channel method). The image of the ratio $I(600\ \text{nm})/I(448\ \text{nm})$ is shown in (d). Red corresponds to the highest intensity; yellow and green, to successively lower intensities; and blue and black indicate the lowest values, as indicated in the color bars.

measurements are indicated, and the ratio $I(600\ \text{nm})/I(448\ \text{nm})$ values between the fluorescence intensities at these wavelengths are shown. Such a ratio, which can vary widely as shown in Fig. 4, yields a first, rough, indication of the spectral shape. This procedure loses the intensity information but has some advantages, which we discuss below.

Spectral signatures from seven different samples of biodeteriogens are shown on a normalized scale in Fig. 5 as recorded remotely by the fluorescence lidar system. Species growing on the facades include green algae from the *Chaetophorales* taxa and the lichens *Scoliciosporum umbrinum*, *Lepraria lobificans*, and *Lecanora dispersa* sp. *lat*. Facade areas with a reasonably dense colonization of particular species were selected to reduce the background fluorescence that was due to the stone. All spectra show the characteristic peak of chlorophyll *a* at ~680 nm. The intensity falloff toward longer wavelengths differs among species; some species even exhibit a second peak, at ~705 nm. There are also spectral differences throughout the visible region from violet to red, which correspond to different accessory pigments. The shape differences exhibited in the spectra of Figs. 4 and 5 suggest that it should be possible to classify different areas of a facade on the basis of their fluorescence spectral signatures.

B. Line Scans

As a preparation for two-dimensional imaging, line scans were performed, particularly for investigation of spectral information dynamics. Each spectrum was integrated over 20 laser shots. Figure 6 shows a vertical scan taken on the left side of the northern portal, as indicated in Fig. 1. The intensity of the sandstone fluorescence varies quite strongly along the line. Unambiguous chlorophyll fluorescence signals are manifest in the middle of this vertical scan.

C. Filter Imaging

As a first step in fluorescence imaging, the fluorescence intensity through the 682-nm filter was recorded, as shown at the bottom left of Fig. 1. Because the filter matches the chlorophyll fluores-

cence spectral band, the areas affected by biodeteriogens appear bright. As the laser was quite stable in its output pulse energy and the biodeteriogen signatures are strong, the main features of the image can readily be interpreted, even if there is no compensation for geometrical effects, etc., which are discussed below.

Figures 7(a) and 7(b) show two images of the portal area [Fig. 7(c)] obtained simultaneously with two-channel detection at 448 and 600 nm, respectively. In the same way as it was possible to identify chlorophyll by its strong red intensity increase in single-wavelength imaging (Fig. 1), it is possible to identify the area of stone iron-ion-fluorescence quenching in each monochrome image, because of strong intensity reductions. In some cases the individual stones are discernible because of the mortar, which has strongly different fluorescence characteristics that compensate for the lacking geometrical resolution.

By forming the ratio $I(600\ \text{nm})/I(448\ \text{nm})$ between the signals of the two channels, one obtains a dimensionless quantity. Such a quantity is independent of the changes in distance and incidence angle, of the fluctuations of the laser pulse energy, and of (wavelength-independent) changes in the detection system's efficiency.

The ratio image [Fig. 7(d)] is therefore sensitive only to the physical and chemical characteristics of the surface and not to its geometry. The suppression of geometrical effects is particularly evident about the door. The intensity ratio changes by a factor of 2 from the flat surface of the portal (mostly 19th-century stone) and the area of ornamented 12th-century stone between the arch and the top of the door. Because only two wavelengths are used, the interpretation can be ambiguous. For instance, if a red filter image (as in Fig. 1) and a blue filter image are recorded for subsequent formation of a ratio image, clean stones, whose fluorescence falls off more slowly toward the red than is normally the case, could be interpreted as areas with small quantities of chlorophyll. It can also be noted that the door appears similar to stone in Fig. 7(d). As a conclusion, the limitations of the two-wavelength method suggest the use of multispectral imaging and advanced statistical information retrieval methods, such as principal–component analysis (PCA).

D. Multispectral Imaging

In PCA analysis[27,28] the total spectral information contained in the image is projected onto an orthogonal set of spectral eigenvectors, which are chosen in such a way that the first eigenvector describes as much as possible of the covariance among the samples. The second eigenvector describes as much as possible of the residual covariance, and so on until all samples are included in the set of orthogonal eigenvectors. If a sufficient number of eigenvectors are used, each individual sample, here each spectrum in the scene recorded, can be reconstructed by a linear combination of the eigenvectors. The eigenvectors are called principal components (PCs); and the expansion coefficients, the scores.

A fluorescence spectrum was detected in each of the 6400 points of the cathedral portal image. The data were then analyzed with a commercial program package for multivariate statistical analysis (The Unscrabler, CAMO ASA, Norway).[28] The multivariate analysis was restricted to the PCA outlined above.

Because the chlorophyll signature is quite different from the other spectral features and in this case is connected to biodeteriogens rather to the building material, it is useful to perform the spectral analysis in three steps, as follows.

In the first step, all the pixels that showed the chlorophyll fluorescence signature were isolated. The criterion used was that the integrated area of the chlorophyll signal should be more than 0.3% of the integrated fluorescence signal (the area under the full fluorescence curve). A polynomial fit to the sloping stone fluorescence background was used to separate the chlorophyll signal. Approximately 25% of the pixels fulfilled this criterion. The criterion was found to be sufficiently robust to pixel noise.

In a second step a PCA analysis was performed on the pixels selected in the first step and including only wavelengths longer than 650 nm. Before this analysis was made, the selected biodeteriogen spectra were corrected for the sloping stone fluorescence background with the fit procedure just described. In this way a full orthogonalization between biodeteriogens and other materials was achieved. The result of this analysis is shown in Fig. 8. In the upper left-hand quadrant the chlorophyll integral value is shown in a gray-scale image. The upper right-hand quadrant shows the shapes of the first two principal components (PC1 and PC2) as determined from the data. As expected, PC1 exhibits a strong peak at 680 nm, the main chlorophyll fluorescence signal. Some addition of the PC2 shape is needed to describe chlorophyll signals with a slow long-wavelength falloff (a positive addition of PC2 lowers the short-wavelength signal and increases the long-wavelength signal). If a sufficient amount of PC2 is added to PC1, a free-standing second peak emerges, as shown in one of the two experimental spectra included in Fig. 8 (corrected for the sloping stone fluorescence background; see also Fig. 5, sample 5). The spatial distribution of the expansion coefficients (scores) is shown as two gray-scale images of the portal (PC1 in the lower-left-hand quadrant; PC2 in the final quadrant.

Biodeteriogen colonization has occurred mostly on the cathedral wall behind the portal addition, related to the more-protected and moister environments found there compared with the exposed portal facade. Small scattered islands of growth were also found on other locations. The PC1 component is the more prominent in all the biodeteriogen pixels, but we also note that most pixel spectra need a PC2 contribution, corresponding to biodeteriogen spectral signatures with a slower slope toward the infrared. Exceptions are found on the two pillar capital fronts, which are dominated by species with strong PC1 signatures.

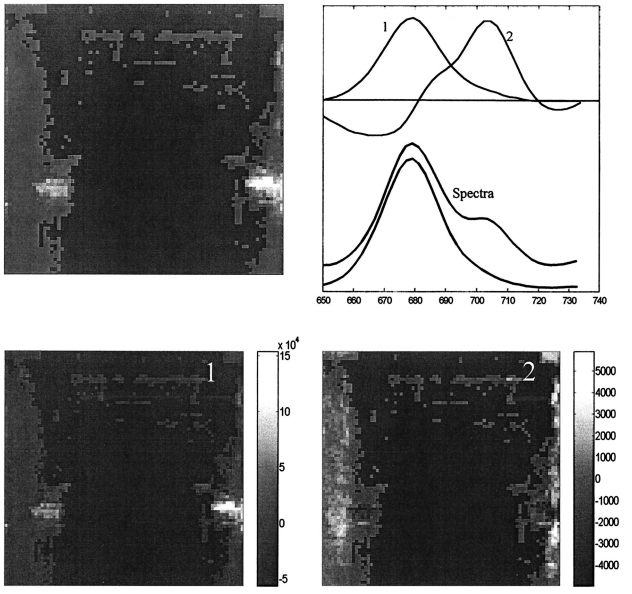

Fig. 8. Demonstration of chlorophyll imaging. All pixels that contain even a minimal chlorophyll signal have been selected and are indicated in gray shades (top left). A PCA is performed in the spectral region 650–740 nm for the chlorophyll signal feature, separated from the sloping stone fluorescence background. The two first PC vectors (PC1 and PC2) for the spectral material are shown at the top right, together with two examples of detected spectra. Finally, images of the scores of the two principal components are shown in gray scale: PC1 (bottom left) and PC2 (bottom right). Here higher intensity is indicated by a lighter color.

Thus the PC2 score image features an intensity reduction in those areas.

Excluding the biodeteriogen pixels from the analysis of the remaining areas reduces the risk of confusing stone fluorescence signatures with the blue–green fluorescence from biodeteriogen assessory pigments.

In the third step, a PC analysis was performed on the nonbiodeteriogen spectra/pixels. Figure 9 shows the first three principal components found and the score plots for PC2 versus PC1 and PC3 versus PC1.

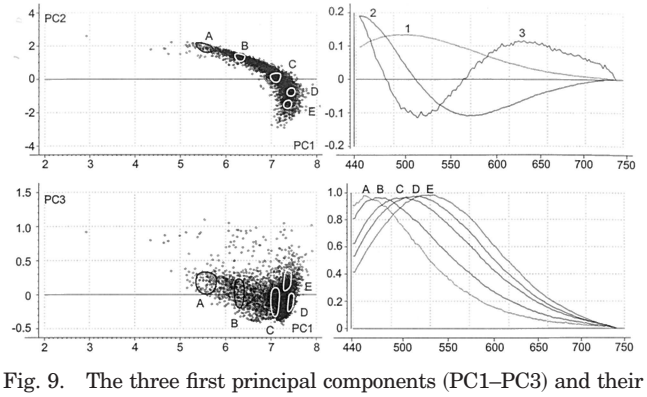

Fig. 9. The three first principal components (PC1–PC3) and their normalized score plots for all nonchlorophyll pixels. The individual spectra can be expressed as a weighted sum of principal components. The averaged spectral shapes from five characteristic locations along the PC2–PC1 and PC3–PC1 score plots are shown (A–E).

Five spectral shapes, averaged for the pixels that belong to the areas marked A–E in the PC2–PC1 and PC3–PC1 plots, are included in the figure. We recognize the shape of the pure PC1 eigenvector in the C area spectrum, whereas the other spectra have positive and negative contributions of PC2, shifting the intensity maximum toward blue and red, respectively.

The data in Fig. 9 correspond to normalized spectra. By using normalized data we secured the analysis from artifacts, as only spectral shape matters. In Fig. 10 a corresponding fully processed false color image of the whole scene is shown. We have merged the biodeteriogen data, whose interpretation is particularly straightforward and which have already been commented on, in their normalized version into Fig. 10, using three shades of red. Pixels with a high biodeteriogen PC1 score (sharp peak at 680 nm) are shown in light red, those with a high biodeteriogen PC2 score in darker red, and those with low values of both PC1 and PC2 scores (indicating little biodeteriogen colonization) with a very dark red color. It is easy to identify the violet area that indicates iron-ion fluorescence quenching because of the sharply falling-off intensity toward the red. It should be noted, though, that this area is even easier to recognize in nonnormalized data because of the very low signal intensity (see Fig. 4, top, and Fig. 7).

The ornamented 12th-century arched stone can be partly discriminated from the 19th-century portal facade stone. Areas related to the particular spectral signatures are shown in blue–indigo and green, respectively.

Multispectral imaging with a PCA interpretation does not require great knowledge of the target spectral features before one starts a measurement. By contrast, when one is using a limited number of receiving filter channels this knowledge is necessary to enable the channels' optimal spectral position to be chosen. The PCA analysis of the spectral signatures can also reveal information that is hidden from the eye. The ability to identify and distinguish different objects can be reduced because of the high signal levels of some objects in the target. Therefore, data are frequently normalized, as demonstrated in connection with Fig. 10.

5. Conclusions

Although further investigations are necessary, the experimental results have clearly demonstrated the feasibility of full-daylight, remote fluorescence imaging of architectural monuments, which could provide assessment of surface damage and help in restoration planning. Two imaging techniques were tested, both successfully. The usefulness and general applicability of principal-component analysis in improving image processing has been demonstrated. The results have also confirmed the possibility of achieving, in practical field work,

- Early detection of biodeteriogens before their presence can be observed with other techniques. It

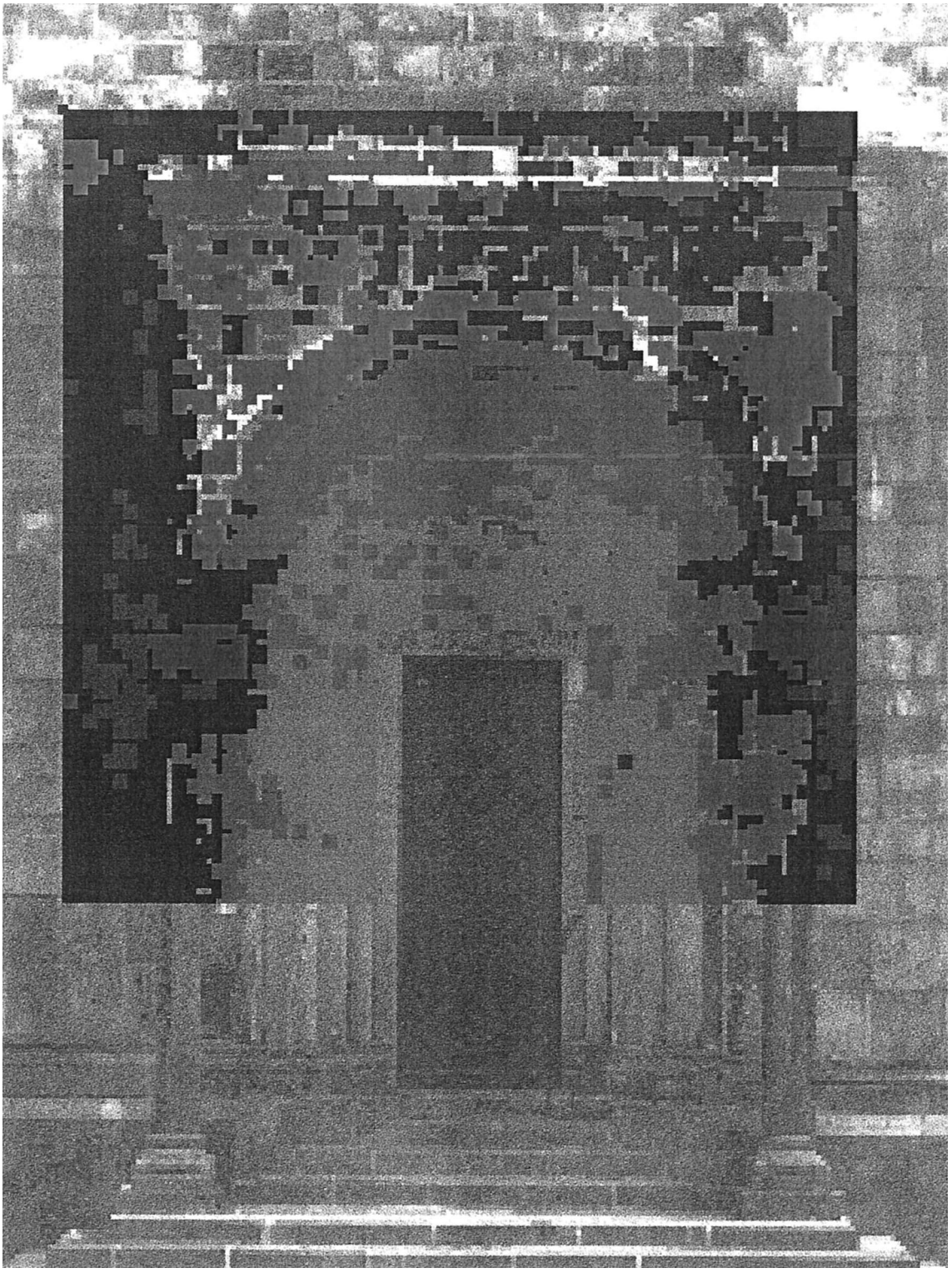

Fig. 10. False-colored image with pixels superimposed upon a photograph of the northern portal. Areas with different characteristics can be identified. Thus, pixels with 12th-century stone characteristics are shown in blue–indigo, and those with 19th-century characteristics are shown in green. The violet pixels correspond to areas that exhibit iron-ion quenching. The normalized chlorophyll pixels from Fig. 8 have been merged in red color tones: Pixels with a large amount of biodeteriogen PC1 are light red; those with a high PC2 score, darker red; and those with both PC1 and PC2 low are shown in a very dark red color.

is important to note that, whereas biodeteriogen colonization on certain areas, such as the sculptures, was visually observable, such was not the case for other areas for which extensive colonizations were clearly detected by both methods.

- Identification of the different stone types, which also opens interesting perspectives for reconstruction of the building's history.

The experiment was carried out without problems, in spite of unfavorable weather conditions. The images of the portal were taken at a distance of ~60 m, but the signal-to-noise ratio obtained during the experiment suggests that detection in full sunlight should still be feasible for at least at a distance of 100 m. Clearly, the capabilities of fluorescence techniques are further enhanced at the low ambient-light levels at night, and useful ranges up to 200 m can be expected.

The results of this research show that remote fluorescence imaging with this new lidar technology is technically practicable. However, additional research is still needed to refine the methodology and to define the data-assessment problems. Progress in solving these problems will require a close interaction between physicists in the remote-sensing field and scientists in the cultural heritage field. In particular, the identification and mapping of facade stone treatment and conservation is a field that shows great promise.[29] Early laboratory work and field monitoring indicate that a considerable potential exists. The study presented here establishes a useful proof of concept from which the newly emerging technology can develop.

This research was supported by the European Community under Access to Large-Scale Facility contract ERB FMGE CT950020 (DG12), by the Swedish National Space Board, the Knut and Alice Wallenberg Foundation, and the Consiglio Nazionale delle Richerche (Italy) Special Project on Science and Technology for Cultural Heritage. The authors are grateful to L. Fröberg for making biological identifications. The kind assistance of and collaboration by E. Cinthio and the personnel of the Lund Cathedral are also gratefully acknowledged.

References

1. E. R. Menzel, *Laser Detection of Fingerprints*, 2nd ed. (Marcel Dekker, New York, 1999).
2. V. Zafiropulus and C. Fotakis, "Lasers in the conservation of painted artwork," in *Laser Cleaning in Conservation: an Introduction*, M. Cooper, ed. (Butterworth Heinemann, Oxford, 1998), Chap. 6.
3. S. Andersson-Engels, C. af Klinteberg, K. Svanberg, and S. Svanberg, "*In vivo* fluorescence imaging for tissue diagnosis," Phys. Med. Biol. **42,** 815–824 (1997).
4. K. Svanberg, I. Wang, S. Colleen, I. Idvall, C. Ingvar, R. Rydell, D. Jocham, H. Diddens, S. Bown, G. Gregory, S. Montán, S. Andersson-Engels, and S. Svanberg, "Clinical multi-colour fluorescence imaging of malignant tumours—initial experience," Acta Radiol. **38,** 2–9 (1998).
5. R. M. Measures, *Laser Remote Sensing: Fundamentals and Applications* (Wiley, New York, 1984).
6. R. A. O'Neill, L. Buja-Bijunas, and D. M. Rayner, "Field performance of a laser fluorosensor for the detection of oil spills," Appl. Opt. **19,** 863–870 (1980).
7. M. Bazzani, B. Breschi, G. Cecchi, L. Pantani, D. Tirelli, G. Valmori, P. Carlozzi, E. Pelosi, and G. Torzillo, "Phytoplankton monitoring by laser induced fluorescence," EARSeL Adv. Remote Sens. **1,** 106–110 (1992).
8. L. Alberotanza, P. L. Cova, C. Ramasco, S. Vianello, M. Bazzani, G. Cecchi, L. Pantani, V. Raimondi, P. Ragnarson, S. Svanberg, and E. Wallinder, "Yellow substance and chlorophyll monitoring in the Venice Lagoon using laser-induced fluorescence," EARSeL Adv. Remote Sens. **3,** 102–110 (1995).
9. H. Edner, J. Johansson, S. Svanberg, E. Wallinder, M. Bazzani, B. Breschi, G. Cecchi, L. Pantani, B. Radicati, V. Raimondi, D. Tirelli, G. Valmori, and P. Mazzinghi, "Laser-induced fluorescence monitoring of vegetation in Tuscany," EARSeL Adv. Remote Sens. **1,** 119–130 (1992).
10. A. Rosema, G. Cecchi, L. Pantani, B. Radicati, M. Romoli, P. Mazzinghi, O. Van Kooten, and C. Kliffen, "Monitoring photosynthetic activity and ozone stress by laser induced fluorescence in trees," Int. J. Remote Sens. **13,** 737–751 (1992).
11. V. Raimondi, G. Cecchi, L. Pantani, and R. Chiari, "Fluorescence lidar monitoring of historical buildings," Appl. Opt. **37,** 1089–1098 (1998).
12. H. Edner, J. Johansson, S. Svanberg, and E. Wallinder, "Fluorescence lidar multicolor imaging of vegetation," Appl. Opt. **33,** 2471–2479 (1994).
13. H. Edner, J. Johansson, P. Ragnarson, S. Svanberg, and E. Wallinder, "Remote monitoring of vegetation using a fluorescence lidar system in spectrally resolving and multi-spectral imaging modes," EARSeL Adv. Remote Sens. **3,** 193–206 (1995).
14. J. Johansson, M. Andersson, H. Edner, J. Mattsson, and S. Svanberg, "Remote fluorescence measurements of vegetation spectrally resolved and by multi-colour fluorescence imaging," J. Plant Physiol. **148,** 632–637 (1996).
15. V. Raimondi, P. Weibring, G. Cecchi, H. Edner, T. Johansson, L. Pantani, B. Sundnér, and S. Svanberg, "Fluorescence imaging of historical buildings by lidar remote sensing," in *Earth Surface Remote Sensing II*, G. Cecchi and E. Zilioli, eds., Proc. SPIE **3496,** 15–20 (1998).
16. H. Edner, K. Fredriksson, A. Sunesson, S. Svanberg, L. Unéus, and W. Wendt, "Mobile remote sensing system for atmospheric monitoring," Appl. Opt. **26,** 4330–4338 (1987).
17. P. Weibring, M. Andersson, H. Edner, and S. Svanberg, "Remote monitoring of industrial emissions by combination of Lidar and plume velocity measurements," Appl. Phys. B **66,** 383–388 (1998).
18. S. Svanberg, "Fluorescence lidar monitoring of vegetation status," Phys. Scr. **T58,** 79–85 (1995).
19. R. Löfvendahl, B. Sundner, *The Lund Cathedral. Stony Material and Damage Assessment* (Central Board for National Antiquities, Stockholm, Sweden, 1997; in Swedish).
20. P. Johansson, *The Lichen Flora on the Lund Cathedral* (Central Board for National Antiquities, Stockholm, Sweden, 1992; in Swedish).
21. P. Johansson, "The lichen flora on the Lund Cathedral," Sven. Botan. Tidskr. **87,** 25–30 (1993).
22. L. Celander, K. Fredriksson, B. Galle, and S. Svanberg, "Investigation of laser-induced fluorescence with applications to remote sensing of environmental parameters," Göteborg Institute of Physics Rep. GIPR-149 (Chalmers University of Technology, Göteborg, Sweden, 1978).
23. S. Svanberg, "Laser fluorescence spectroscopy in environmental monitoring," in *Optoelectronic for Environmental Science*, S. Martellucci and A. N. Chester, eds. (Plenum, New York, 1990), pp. 15–27.
24. G. Cecchi, L. Pantani, V. Raimondi, D. Tirelli, and R. Chiari, "The fluorescence lidar technique for the remote sensing of stony materials in ancient buildings," in *Remote Sensing for*

Geography, Geology, Land Planning, and Cultural Heritage, D. Arroyo-Bishop, R. Carla, J. B. Lurie, C. M. Marino, A. Panunzi, J. J. Pearson, and E. Zioli, eds., Proc. SPIE **2960,** 163–172 (1996).
25. G. Cecchi, L. Pantani, V. Raimondi, D. Tirelli, R. Chiari, L. Tomaselli, G. Lamenti, M. Bosco, and P. Tiano, "Fluorescence lidar technique for the monitoring of biodeteriogens on the cultural heritage," in *Remote Sensing for Geography, Geology, Land Planning, and Cultural Heritage*, D. Arroyo-Bishop, R. Carla, J. B. Lurie, C. M. Marino, A. Panunzi, J. J. Pearson, and E. Zioli, eds., Proc. SPIE **2960,** 137–146 (1996).
26. A. S. Marfunin, *Spectroscopy, Luminescence, and Radiation Centers in Minerals* (Springer-Verlag, Berlin, 1979).
27. K. R. Beebe and B. Kowalski, "An introduction to multivariate calibration and analysis," Anal. Chem. **59,** 1607A (1987).
28. K. Esbensen, T. Midtgaard, S. Schonkopf, and D. Guyoyf, *Multivariate Analysis—A Training Package* (CAMO ASA, Oslo, Norway, 1994).
29. G. Ballerini, S. Bracci, L. Pantani, and P. Tiano, "Lidar remote sensing of stone cultural heritage: detection of protective treatments," Opt. Eng. **40,** 1579–1583.